

Supplementary Materials for

Neurotoxic peptides from the venom of the giant Australian stinging tree

Edward K. Gilding, Sina Jami, Jennifer R. Deuis, Mathilde R. Israel, Peta J. Harvey, Aaron G. Poth, Fabian B. H. Rehm, Jennifer L. Stow, Samuel D. Robinson, Kuok Yap, Darren L. Brown, Brett R. Hamilton, David Andersson, David J. Craik, Irina Vetter*, Thomas Durek*

*Corresponding author. Email: i.vetter@uq.edu.au (I.V.); t.durek@uq.edu.au (T.D.)

Published 16 September 2020, *Sci. Adv.* **6**, eabb8828 (2020)

DOI: [10.1126/sciadv.abb8828](https://doi.org/10.1126/sciadv.abb8828)

This PDF file includes:

Supplementary Materials and Methods

Figs. S1 to S6

References

Supplementary Materials and Methods

RNA-seq data analysis

Data were assessed for quality using FastQC (Barambam Software) before being trimmed using Trimmomatic (29) and assembled with Trinity (30). Parameters for trimming and assembly of data are given below.

Trimmomatic parameters:

```
ILLUMINACLIP:Adaptors NovaSeq.fa:2:30:10 HEADCROP:14 TRAILING:30  
MINLEN:30
```

Trinity parameters:

```
--KMER SIZE 27 --min kmer cov 2 --path reinforcement distance 30
```

Primers used for cDNA cloning

<u>Primers for amplification of Dendrocnide Sequences</u>		
<u>Primer name</u>	<u>Sequence (5' → 3')</u>	<u>Target amplicon</u>
ExTxA_for	ATG AGG TTT GCA CTA GTT GCG G	
ExTxA_rev	TTA CAC ATC GGG AAC ACA AAG TCC	Excelsatoxin A CDS
ExTxB_for	ATG GCA GCA GTG AAG AAG CAT ATG AG	
ExTxB_rev	TTA CCC GTT GGG AAT ACA AAA TCC	Excelsatoxin B CDS
MoTxA_for	ATG GCA GCA GTG AAG AAG CAT	
MoTxA_rev	TTA CAC ACT GGG AAC ACA AAT TCC	Moroidotoxin A CDS

Primers used for cloning PCR products were identical to those in the table above except had attB GatewayTM sites

incorporated at their 5' termini (5' → 3' attB1: GGG GAC AAG TTT GTA CAA AAA AGC AGG CT and attB2:

GGG GAC CAC TTT GTA CAA GAA AGC TGG GT).

Peptide synthesis:

Gympietides were chemically synthesized by automated Fmoc SPPS using optimized protocols. The peptides were assembled on 2-chlorotrityl chloride resin using the following side chain protecting groups: Asp(tBu), Lys(Boc), Arg(Pbf), Ser(tBu), and Thr(tBu). Resin cleavage and side-chain deprotection were carried out by suspending the dried peptide-resin in cleavage cocktail (TFA:triisopropylsilane:H₂O; 95:2.5:2.5). After stirring for 1.5 h at room temperature, the majority of TFA was evaporated under reduced pressure and the peptide was precipitated with ice-cold diethyl ether. The peptide was dissolved in 50% ACN/water containing 0.05% TFA and lyophilized. Crude peptides were dissolved in a 10% (v/v) ACN-water mixture containing 0.05% (v/v) TFA, before being purified by preparative rpHPLC. The column was equilibrated with 10% of solvent B (ACN:H₂O:TFA; 89.95:10:0.05) in solvent A (H₂O:TFA; 99.95:0.05). Peptides were eluted using linear gradients of solvent B in solvent A, and fractions were collected across the expected elution time. Peptide purity and identity were assessed by ESI-MS on Shimadzu 2020 LC mass spectrometer and by analytical scale UPLC on a Shimadzu Nexera system equipped with an Agilent Zorbax C18 column (1.8 mm, 2.1 x 100 mm). Fractions containing the desired product were pooled, lyophilized and stored at -20 °C. Observed masses: m/z 972.4 [M+4H]⁴⁺; m/z 1296.1 [M+3H]³⁺ (ESI-MS); calculated masses (average isotope composition): m/z 972.4 [M+4H]⁴⁺; m/z 1296.2 [M+3H]³⁺.

Folding and disulfide formation were carried out by incubating the reduced peptides in folding buffer (200 mM ammonium bicarbonate, 55% (v/v) isopropanol, 5 mM reduced glutathione, 0.5 mM oxidized glutathione, pH 8.2) at a peptide concentration of 0.2 mg/mL. After stirring at 23 °C for 16-24 h the products were isolated by preparative rpHPLC as described above. Observed

monoisotopic mass: m/z 3877.80 $[M+H]^+$ HR-MALDI-MS (CHCA); calculated monoisotopic mass: m/z 3877.88 $[M+H]^+$.

Peptide identification via tandem MS

Peptides were dissolved in 100 mM NH_4HCO_3 , pH 7.8, before dithiothreitol (DTT) was added to a final concentration of 10 mM for the reduction of disulfide bonds. The mixture was incubated at 60°C for 30 minutes. The reduced peptides were alkylated by the addition of iodoacetamide (IAA) to a final concentration of 25 mM and the mixture was left at room temperature for 30 minutes. Reduced and alkylated peptides were treated with trypsin and left overnight at 37°C. The reaction was quenched by the addition of formic acid to a final concentration of 1% (v/v). Samples were then analysed on a Shimadzu UPLC interfaced with a SCIEX TripleTOF® 5600+ using information dependent acquisition (IDA) scanning. Experiments were conducted using an Agilent Zorbax C18 UPLC column 300Å (100 x 2.1 mm, 1.8 µm) maintained at 60°C using a linear acetonitrile gradient at a flow rate of 200 µL/min. Ion spray voltage was set at 5500 V, source temperature at 500°C and IDA scans were performed with unit resolution in Q1. SCIEX Analyst software was used for data analysis.

Quantification of acetylcholine, histamine, serotonin and ExTxA via targeted UPLC-MS-MRM

Histamine and serotonin (5-HT) were analyzed after derivatization with benzoylchloride while acetylcholine and ExTxA were analyzed directly from extracts without further modification (31). For derivatization, 50 µL of standard or sample was mixed with 25 µL of 100 mM sodium tetraborate buffer (pH 9.5) and 25 µL of benzoyl chloride solution (2 % (v/v) in acetonitrile). The reaction was left at 23°C for 30 min. After centrifugation at 10,000 x g for 5 min, the supernatant was removed and used for multiple reaction monitoring (MRM) analysis. The

analytes/compounds were quantified using targeted MRM analyses performed on a SCIEX QTRAP® 6500+ mass spectrometer coupled with a SCIEX Exion UPLC system. Quantification experiments were conducted using a Phenomenex Kinetex C18 UPLC column (100 x 2.1mm, 1.7 µm) maintained at 60°C using a linear acetonitrile gradient at a flow rate of 400 µL/min. Ion spray voltage was set at 4500-5500 V, source temperature at 600°C and MRM scans were performed with low resolution in Q1 and unit resolution in Q3. SCIEX MultiQuant software was used for data analysis.

The following parameters were used for quantitative experiments:

Analyte	Q1 (m/z)	Q3 (m/z)	Collision energy (V)	Declustering potential (eV)
ExTxA	970.0	963.3	40.0	60.0
serotonin	385.1	264.1	30.0	70.0
histamine	216.1	105.3	30.0	70.0
acetylcholine	146.2	87.2	30.0	70.0

For qualitative ExTxA determination (**Fig. S3**), the following transition ions were monitored:

Transition	Q1 (m/z)	Q3 (m/z)	Collision Energy (V)	Declustering potential (eV)
1	970.0	963.3	40.0	60.0
2	970.0	1244.2	42.0	60.0
3	970.0	1223.2	44.0	60.0
4	970.0	1174.1	46.0	60.0
5	970.0	330.1	53.0	60.0
6	970.0	1284.1	65.0	60.0
7	970.0	1174.5	67.0	60.0
8	970.0	1761.0	74.0	60.0
9	970.0	1820.7	77.0	60.0
10	970.0	1427.2	75.0	60.0

Matrix assisted laser desorption ionization imaging mass spectrometry (MALDI-IMS).

To prepare sections for MALDI-IMS, fresh petioles of *Dendrocnide excelsa* were cut transversely and longitudinally with a scalpel into pieces of approximately 10 mm. The samples were embedded in ice by suspending them in distilled water and freezing at -80°C. The ice-

embedded samples were cut from the block using a Leica CM 3050S cryostat to obtain sections with a thickness of 25 μm . The sections were transferred to Indium Tin Oxide (ITO)-coated glass slides (Bruker Daltonik), briefly washed with ice-cold distilled water and dried at room temperature. Light microscopy images were obtained with an Olympus SZX12 microscope equipped with an Olympus DP70 digital camera.

For MALDI-IMS analysis the ITO glass slides were sprayed with a matrix solution of α -cyano-4-hydroxycinnamic acid (CHCA, 7 mg/mL in 50% acetonitrile (aq) with 0.2% TFA) using a Bruker ImagePrep device. Optical images of the sprayed slides were collected and the slides were loaded into a Bruker Ultraflex III MALDI-TOF/TOF mass spectrometer, controlled by Flex Control 3.3 and Flex Imaging 4.0. The imaging mass spectrometry experiment was performed in linear positive mode over a mass range of m/z 1000 – 10000, with 400 shots acquired at 200 Hz, medium laser size, and calibrated prior to analysis using clinprot standards (Bruker Daltonics). The acquired data was visualized with RMS normalization in Flex Imaging 4.0, and SCILS LAB (2017a).

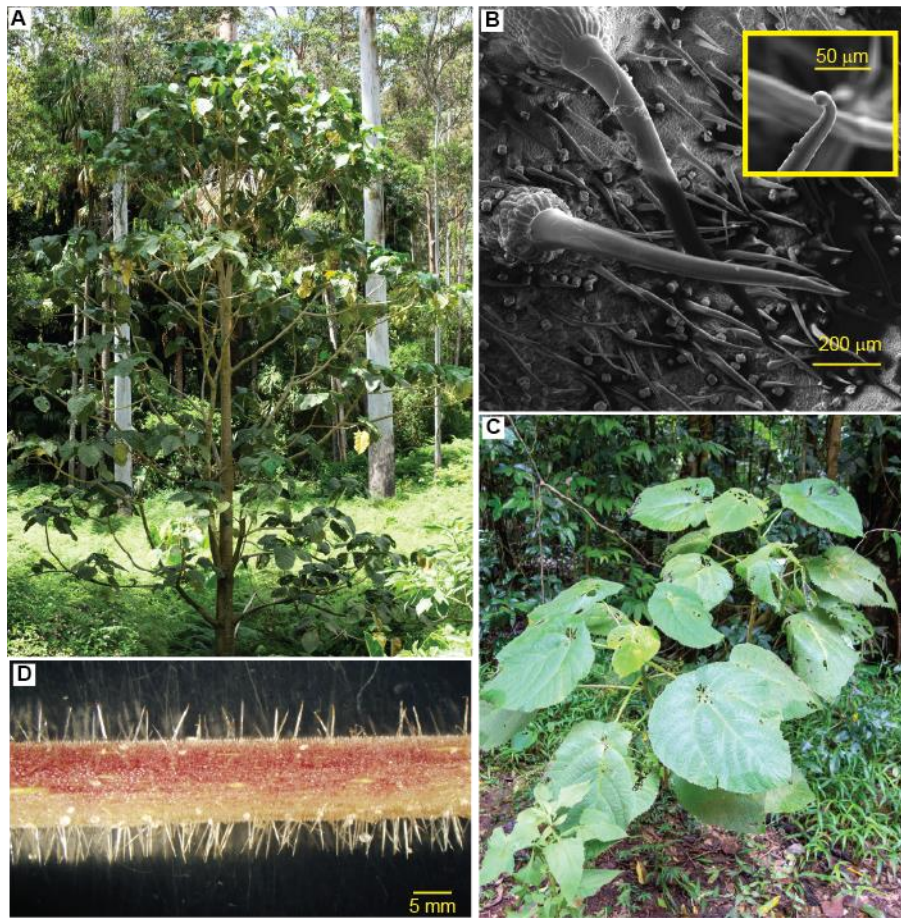


Figure S1: *Dendrocnide excelsa* and *Dendrocnide moroides* in natural habitat. (A) Young *D. excelsa* tree (~ 6-8 m tall) growing in a rainforest clearing near Mount Lindesay in southeast QLD, Australia. (B) SEM image of a young *D. excelsa* leaf. The inset shows a detail view of the barbed trichome tip. (C) *D. moroides* (1.5 m tall) near Cairns, QLD, Australia. (D) Petioles of *D. moroides*.

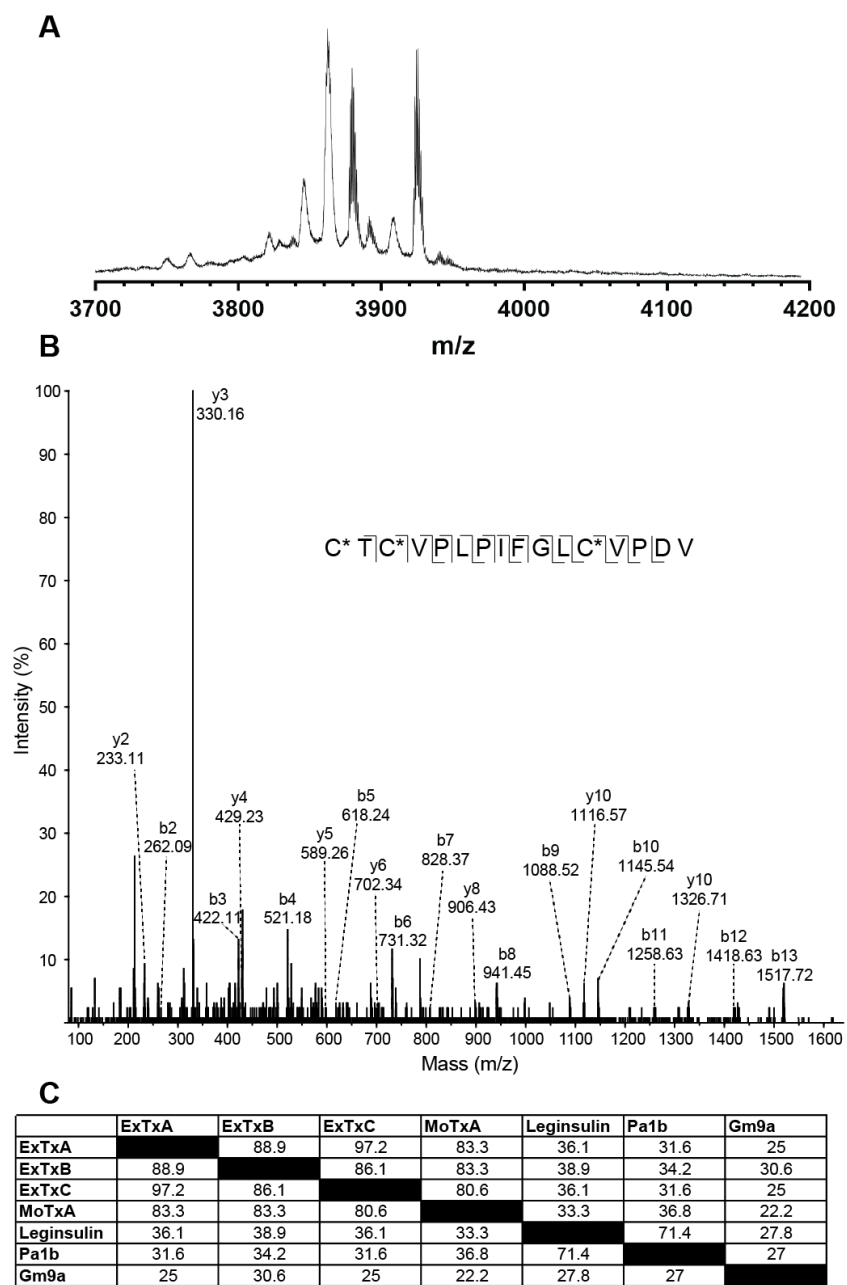


Figure S2: MS characterization of the MS/MS spectrum of ExTxA fragment obtained from the pain-causing *D. excelsa* fraction and sequence analysis (A) MALDI-MS spectrum (B) MS/MS spectrum of ExTxA fragment after reduction and alkylation with iodoacetamide (C* indicates carboxyamidomethylated cysteine) and digestion with trypsin. Precursor ion m/z 923.9²⁺ Da. Assignment of the isobaric Ile and Leu residues was based on the RNAseq (transcriptome) data. (C) Percent identity matrix for the peptides presented in Fig. 2A.

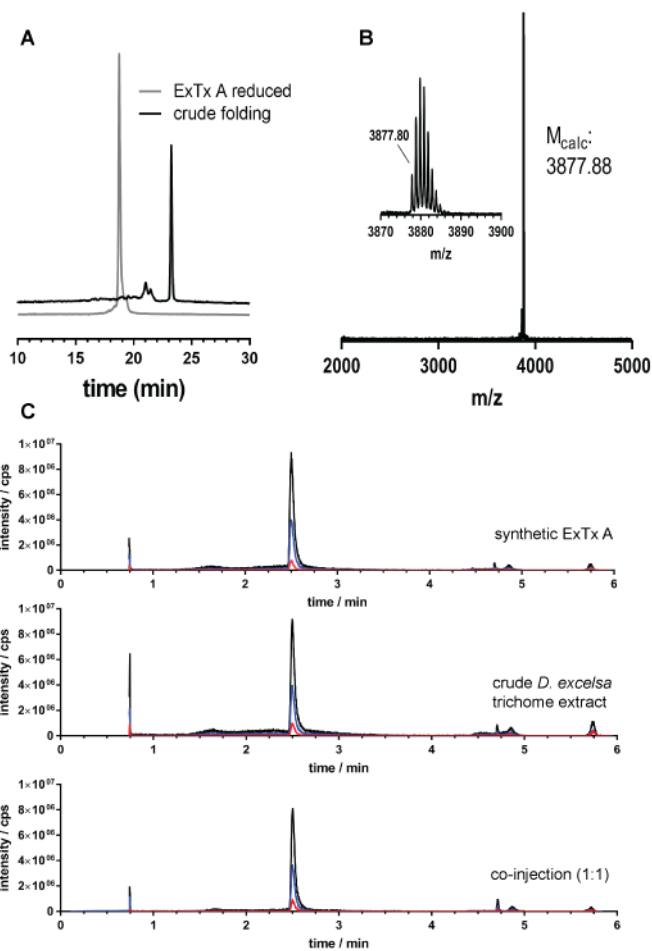


Figure S3: Chemical synthesis and analysis of ExTxA. (A) HPLC analysis of ExTxA *in vitro* folding. (B) High-resolution MALDI-MS spectrum of synthetic ExTxA. (C) UPLC-MS-MRM analysis of synthetic and plant-derived ExTxA. MRM was performed on 10 transition ions (see supplementary methods above). Only the three most prominent transitions are shown here (black: 970 \rightarrow 963; blue: 970 \rightarrow 1244; red: 1293 \rightarrow 1284).

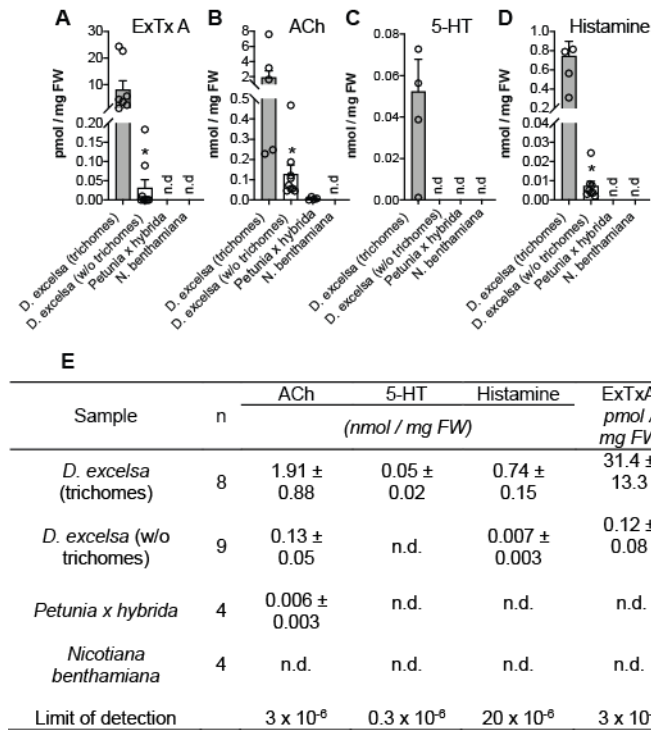


Figure S4: Quantitative analysis of small molecule neurotransmitters/inflammatory mediators and ExTxA in plant tissues. (A) ExTxA; (B) acetylcholine (ACh); (C) 5-hydroxytryptamine (5-HT); (D) histamine; (E) Values given are mean ± standard error of the mean of n biological replicates. Each n is the average of three technical replicates. n.d.: not detected (below limit of detection); FW: fresh weight.

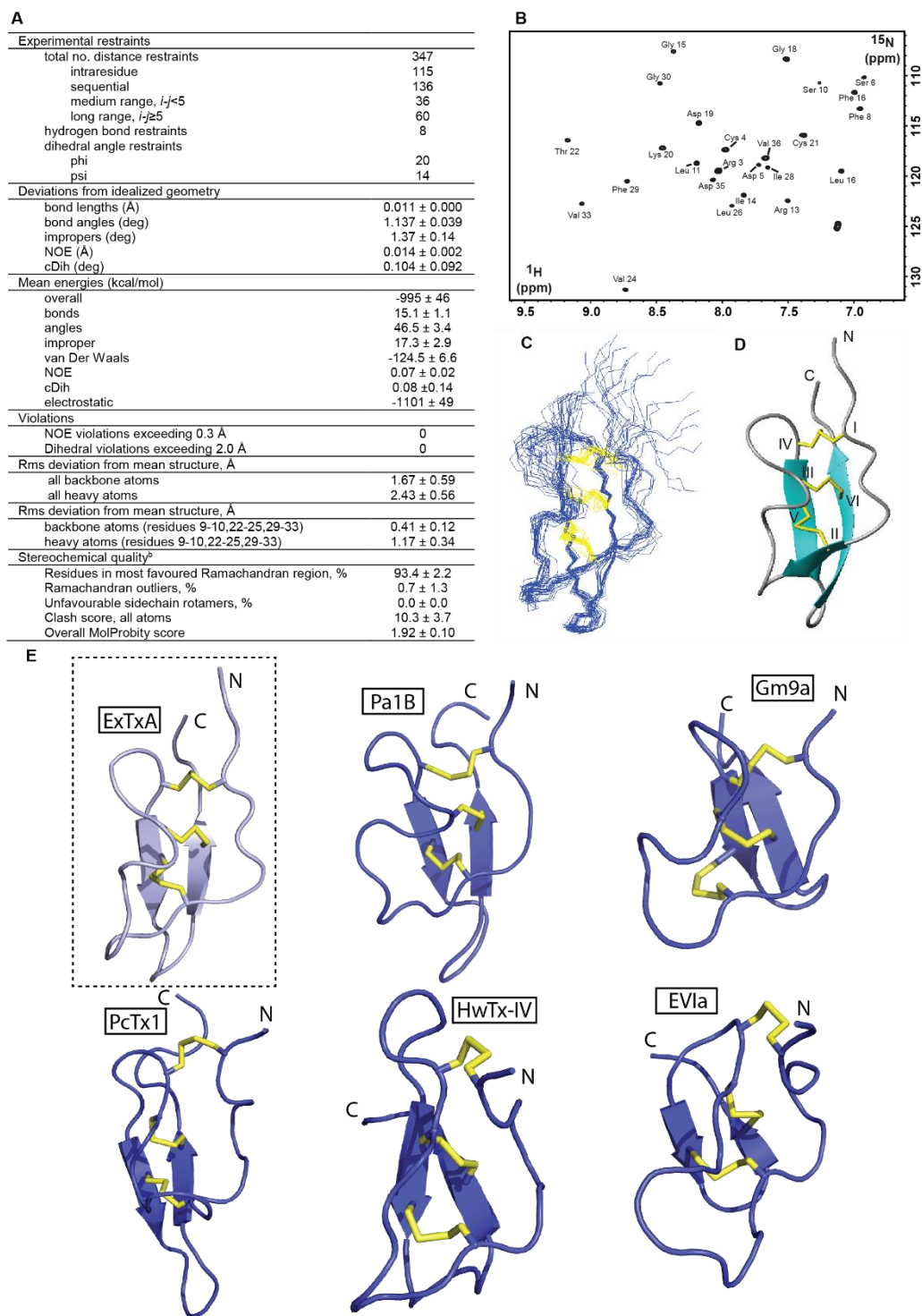


Figure S5: NMR analysis of synthetic ExTxA. (A) Statistical analysis of ExTxA structures. All values are given as mean ± standard deviation. (B) Natural abundance ^1H - ^{15}N -HSQC spectrum acquired at 600 MHz, 40 % (v/v) ACN- D_3 in water, 298 K. (C) Overlay of backbone atoms

(blue) and disulfide bonds (yellow) of the 20 lowest energy calculated structural models of ExTxA. **(D)** Ribbon representation showing secondary structure elements and disulfide connectivity. **(E)** 3D structure comparison of representative ICK peptides (clockwise from top left): ExTxA (*Dendrocnide excelsa*, PDB ID: 6VH8), Pa1B (*Pisum sativum*, PDB ID: 1P8B), Conotoxin Gm9a (*Conus gloriamaris*, PDB ID: 1IXT), δ -Conotoxin EVIa (*Conus ermineus*, PDB ID: 1G1P), spider toxin Huwentoxin-IV (*Selenocosmia huwena*, PDB ID: 1MB6), spider toxin PcTx1 (*Psalmopoeus cambridgei*, PDB ID: 1LMM). Disulfide bonds are shown in yellow.

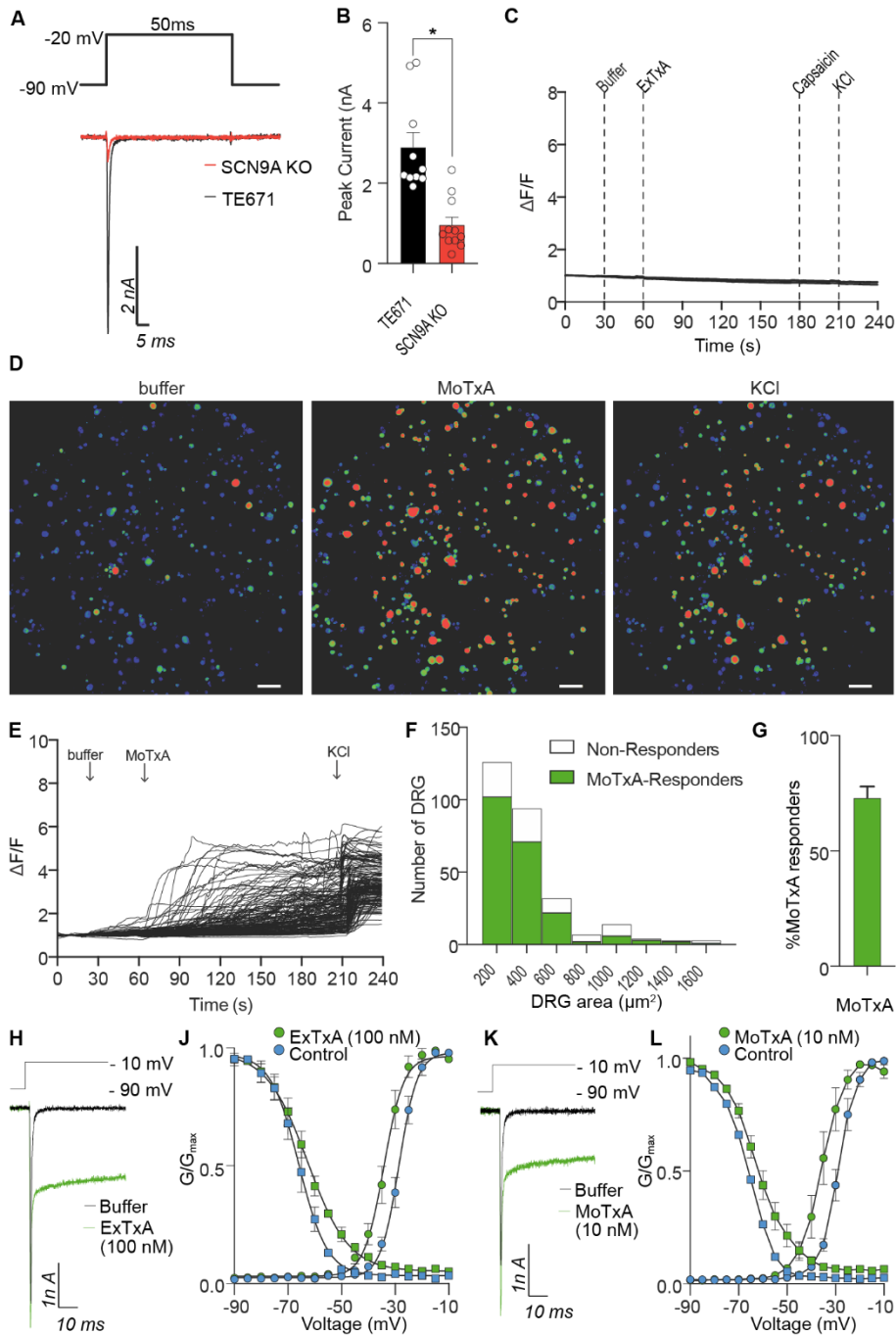


Figure S6: Pharmacological characterization of ExTxA and MoTxA. (A) Nav1.7 mediates endogenous voltage-gated sodium current in TE671 cells. Representative inward sodium current trace in a native TE671 cell (black) overlaid with a current trace from a SCN9A (gene encoding for Nav1.7) KO (knockout) TE671 cell (red). (B) Peak inward sodium current in TE671 cells (n = 10) is significantly (p=0.0001) decreased compared to SCN9A KO-TE671 cells (n = 11). Data

are presented as mean \pm standard error of the mean. Statistical significance was determined using two-tailed t-test, * $p < 0.05$ compared to control. **(C)** ExTxA does not induce calcium influx in non-neuronal cells. Traces from non-neuronal cells ($n = 5$; defined by lack of response to KCl) of one representative experiment. **(D-G)** MoTxA (10 nM) induces Ca^{2+} influx in DRG neurons. **(D)** Pseudocolor images illustrating Ca^{2+} responses in DRG neurons (scale bar, 100 μm), and **(E)** corresponding traces from all neurons of one representative experiment. **(F)** Distribution of MoTxA-responding and non-responding DRG neurons by cell size. **(G)** Total percentage of neurons responding to MoTxA (10 nM). Data are presented as mean \pm S.E.M.; * $p < 0.05$. **(H)** Representative current traces showing that ExTxA (100 nM) delays fast inactivation of voltage-gated Na^+ current in TE671 cells. **(J)** Effect of ExTxA (100 nM, green symbols) on the conductance-voltage (GV) curve of Na^+ current compared to control (blue symbols). Channel activation (circles); steady-state inactivation, squares ($n = 5$). **(K)** Representative current traces showing that MoTxA (10 nM) delays fast inactivation of voltage-gated Na^+ current in TE671 cells. **(L)** Effect of MoTxA (10 nM, green symbols) on the conductance-voltage (GV) curve of Na^+ current compared to control (blue symbols). Channel activation (circles); steady-state inactivation, squares ($n = 5$).

REFERENCES AND NOTES

1. W. F. MacFarlane, The stinging properties of *Laportea*. *Econ. Bot.* **17**, 303–311 (1963).
2. P. A. Robertson, W. V. Macfarlane, Pain-producing substances from the stinging bush *Laportea moroides*. *Aust. J. Exp. Biol. Med. Sci.* **35**, 381–394 (1957).
3. D. Maor, M. Little, Skin contact with a stinging tree requiring intensive care unit admission. *Contact Dermatitis* **77**, 335–337 (2017).
4. C. Schmitt, P. Parola, L. de Haro, Painful sting after exposure to dendrocnide sp: Two case reports. *Wild. Environ. Med.* **24**, 471–473 (2013).
5. A. Mustafa, H.-J. Ensikat, M. Weigend, Stinging hair morphology and wall biomineralization across five plant families: Conserved morphology versus divergent cell wall composition. *Am. J. Bot.* **105**, 1109–1122 (2018).
6. A. J. Cummings, M. Olsen, Mechanism of action of stinging nettles. *Wild. Environ. Med.* **22**, 136–139 (2011).
7. H. Schildknecht, Irritant and defense substances of higher plants—A chemical herbarium. *Angew. Chem. Int. Ed.* **20**, 164–184 (1981).
8. N. Emmelin, W. Feldberg, The mechanism of the sting of the common nettle (*Urtica urens*). *J. Physiol.* **106**, 440–455 (1947).
9. H. O. J. Collier, G. B. Chesher, Identification of 5-hydroxytryptamine in the sting of the nettle (*Urtica dioica*). *Brit. J. Pharmacol. Chemother.* **11**, 186–189 (1956).
10. F. Oliver, E. U. Amon, A. Breathnach, D. M. Francis, P. Sarathchandra, A. K. Black, M. W. Greaves, Contact urticaria due to the common stinging nettle (*Urtica dioica*)—Histological, ultrastructural and pharmacological studies. *Clin. Exp. Dermatol.* **16**, 1–7 (1991).
11. H. Y. Fu, S. J. Chen, R. F. Chen, W. H. Ding, L. L. Kuo-Huang, R. N. Huang, Identification of oxalic acid and tartaric acid as major persistent pain-inducing toxins in the stinging hairs of the nettle, *Urtica thunbergiana*. *Ann. Bot.* **98**, 57–65 (2006).
12. L. A. Miles, C. Y. Dy, J. Nielsen, K. J. Barnham, M. G. Hinds, B. M. Olivera, G. Bulaj, R. S. Norton, Structure of novel P-superfamily spasmodic conotoxin reveals an inhibitory cystine knot motif. *J. Biol. Chem.* **277**, 43033–43040 (2002).
13. J. Bell, A. Seed, *Dictionary of the Gubbi-Gubbi and Butchulla Languages* (J. Bell, 1994), 166 pp.
14. I. Vetter, J. R. Deuis, A. Mueller, M. R. Israel, H. Starobova, A. Zhang, L. D. Rash, M. Mobli, Nav1.7 as a pain target—From gene to pharmacology. *Pharmacol. Ther.* **172**, 73–100 (2017).

15. J. R. Deuis, Z. Dekan, J. S. Wingerd, J. J. Smith, N. R. Munasinghe, R. F. Bhola, W. L. Imlach, V. Herzig, D. A. Armstrong, K. J. Rosengren, F. Bosmans, S. G. Waxman, S. D. Dib-Hajj, P. Escoubas, M. S. Minett, M. J. Christie, G. F. King, P. F. Alewood, R. J. Lewis, J. N. Wood, I. Vetter, Pharmacological characterisation of the highly Na_v1.7 selective spider venom peptide Pn3a. *Sci. Rep.* **7**, 40883 (2017).
16. K. Zimmermann, J. R. Deuis, M. C. Inserra, L. S. Collins, B. Namer, P. J. Cabot, P. W. Reeh, R. J. Lewis, I. Vetter, Analgesic treatment of ciguatoxin-induced cold allodynia. *Pain* **154**, 1999–2006 (2013).
17. H. Morita, K. Shimbo, H. Shigemori, J. Kobayashi, Antimitotic activity of moroidin, a bicyclic peptide from the seeds of *Celosia argentea*. *Bioorg. Med. Chem. Lett.* **10**, 469–471 (2000).
18. P. B. Oelrichs, P. A. Robertson, Purification of pain-producing substances from dendrocnide (*Laportea*) moroides. *Toxicon* **8**, 89–90 (1970).
19. T.-W. C. Leung, D. H. Williams, J. C. J. Barna, S. Foti, P. B. Oelrichs, Structural studies on the peptide moroidin from *Laportea moroides*. *Tetrahedron* **42**, 3333–3348 (1986).
20. D. R. Nelsen, Z. Nisani, A. M. Cooper, G. A. Fox, E. C. K. Gren, A. G. Corbit, W. K. Hayes, Poisons, toxins, and venoms: Redefining and classifying toxic biological secretions and the organisms that employ them. *Biol. Rev.* **89**, 450–465 (2014).
21. M. Hurley, in *Beating Around the Bush* (The Conversation, 2018); <https://theconversation.com/the-worst-kind-of-pain-you-can-imagine-what-its-like-to-be-stung-by-a-stinging-tree-103220>.
22. Y. Shen, A. Bax, Protein backbone and sidechain torsion angles predicted from NMR chemical shifts using artificial neural networks. *J. Biomol. NMR* **56**, 227–241 (2013).
23. A. T. Brünger, P. D. Adams, G. M. Clore, W. L. DeLano, P. Gros, R. W. Grosse-Kunstleve, J.-S. Jiang, J. Kuszewski, M. Nilges, N. S. Pannu, R. J. Read, L. M. Rice, T. Simonson, G. L. Warren, Crystallography & NMR system: A new software suite for macromolecular structure determination. *Acta Crystallogr. D* **54**, 905–921 (1998).
24. V. B. Chen, W. B. Arendall III, J. J. Headd, D. A. Keedy, R. M. Immormino, G. J. Kapral, L. W. Murray, J. S. Richardson, D. C. Richardson, MolProbity: All-atom structure validation for macromolecular crystallography. *Acta Crystallogr. D* **66**, 12–21 (2010).
25. K. Zimmermann, A. Hein, U. Hager, J. S. Kaczmarek, B. P. Turnquist, D. E. Clapham, P. W. Reeh, Phenotyping sensory nerve endings in vitro in the mouse. *Nat. Protoc.* **4**, 174–196 (2009).
26. T. R. Cummins, A. M. Rush, M. Estacion, S. D. Dib-Hajj, S. G. Waxman, Voltage-clamp and current-clamp recordings from mammalian DRG neurons. *Nat. Protoc.* **4**, 1103–1112 (2009).

27. S. D. Robinson, A. Mueller, D. Clayton, H. Starobova, B. R. Hamilton, R. J. Payne, I. Vetter, G. F. King, E. A. B. Undheim, A comprehensive portrait of the venom of the giant red bull ant, *Myrmecia gulosa*, reveals a hyperdiverse hymenopteran toxin gene family. *Sci. Adv.* **4**, eaau4640 (2018).
28. M. C. Inserra, M. R. Israel, A. Caldwell, J. Castro, J. R. Deus, A. M. Harrington, A. Keramidas, S. Garcia-Caraballo, J. Maddern, A. Erickson, L. Grundy, G. Y. Rychkov, K. Zimmermann, R. J. Lewis, S. M. Brierley, I. Vetter, Multiple sodium channel isoforms mediate the pathological effects of pacific ciguatoxin-1. *Sci. Rep.* **7**, 42810 (2017).
29. A. M. Bolger, M. Lohse, B. Usadel, Trimmomatic: A flexible trimmer for illumina sequence data. *Bioinformatics* **30**, 2114–2120 (2014).
30. M. G. Grabherr, B. J. Haas, M. Yassour, J. Z. Levin, D. A. Thompson, I. Amit, X. Adiconis, L. Fan, R. Raychowdhury, Q. Zeng, Z. Chen, E. Mauceli, N. Hacohen, A. Gnirke, N. Rhind, F. di Palma, B. W. Birren, C. Nusbaum, K. Lindblad-Toh, N. Friedman, A. Regev, Full-length transcriptome assembly from RNA-seq data without a reference genome. *Nat. Biotechnol.* **29**, 644–652 (2011).
31. P. Song, O. S. Mabrouk, N. D. Hershey, R. T. Kennedy, In vivo neurochemical monitoring using benzoyl chloride derivatization and liquid chromatography-mass spectrometry. *Anal. Chem.* **84**, 412–419 (2012).